Journal of Photochemistry & Photobiology, A: Chemistry 444 (2023) 114917

Contents lists available at ScienceDirect

Journal of Photochemistry & Photobiology, A: Chemistry

journal homepage: www.elsevier.com/locate/jphotochem

Optimizing the use of light in supported TiO_2 photocatalysts: Relevance of the shell thickness

Oscar Cabezuelo, Ander Diego-Lopez, Pedro Atienzar, M. Luisa Marin *, Francisco Bosca *

Instituto de Tecnología Química, Universitat Politècnica de València-Consejo Superior de Investigaciones Científicas, Avda. de los Naranjos s/n, E-46022, Valencia, Spain

ARTICLE INFO

Keywords:
Heterogeneous photocatalysts
Semiconductor
Crystallite size
Reduced e^--h^+ recombination
Inaccessible e^--h^+ pairs

ABSTRACT

Heterogeneous photocatalysts have attracted significant interest over the last few years. In this sense, improved photocatalytic properties for SiO_2@TiO_2 materials have been correlated with higher semiconductor's specific surface area and adsorption capability. However, the reported TiO_2 shell optimizations did not consider the percentage of the photo-excited electron-hole (e^--h^+) pairs occurring in the inaccessible surface of the TiO_2 shell. The present study aimed to find the best TiO_2 shell thickness for the optimal harvest of light. For this purpose, the sol–gel method was modified by applying a precise humid airflow to get a uniform deposition of titania on the surface of the SiO_2 particles. As a result, photocatalysts with a robust and homogeneous TiO_2 shell of different thicknesses (from 14 to 42 nm) with well-defined particle size for TiO_2 crystals (*ca.* 12 nm) were obtained. The SiO_2@TiO_2 materials were extensively characterized. Finally, their photocatalytic activity was evaluated against methylene blue under irradiation by UVA light. Analysis of the results revealed that the most efficient photocatalyst has a TiO_2 shell thickness of *ca.* 30 nm. Emission and photocurrent studies also agreed with the photocatalytic results suggesting a reduced e^--h^+ recombination rate. Thereby, for the first time, the relevance of shell thickness in supported photocatalysts has been demonstrated.

1. Introduction

The exponential growth of industrial developments, together with the intensive exploitation of agriculture, has led to the uncontrolled release of organic pollutants into natural water, resulting in several environmental problems, such as inadequate access to clean water and sanitation, as one of the most alarming issues at a global scale. In this sense, millions of people die every year from waterborne diseases due to unsafe water and lack of basic sanitation [1]. Recently, many studies have reported the presence of *contaminants of emerging concern* (CECs), such as fungicides, pesticides, and/or endocrine-disrupting chemical residues, in wastewater, surface waters, and ground waters [2–4]. Given this reality, the development of alternative technologies for proper wastewater treatment is required to face water contamination [5,6].

Advanced Oxidation Processes (AOPs), which rely on the formation of highly reactive species to transform recalcitrant organic pollutants into biodegradable compounds, have been proposed as alternative technologies to conventional methods for wastewater treatment. Among them, heterogeneous photocatalysis, which often involves the interaction between light and semiconductors, has been widely reported as a viable option [7–9]. In this sense, titanium dioxide (TiO_2) is a widely recognized photocatalyst with demonstrated efficiency in removing organic pollutants, mainly by forming hydroxyl radical (·OH), although other semiconductors have also been tested [10,11]. Advantages of TiO_2 include chemical stability, lack of toxicity, suitable optical properties like activation in the presence of UV light, and crystallinity, being the anatase phase the most photoactive one [12]. Among the commercial options, Degussa P25 TiO_2 has become the standard of use because of its well-defined crystallinity (80:20 anatase: rutile), surface area (55 ± 15 m^2g^{-1} BET), average particle size (21 nm), and higher photoactivity than other commercial TiO_2 sources [13–15]. Nevertheless, several limitations make its practical applicability problematic and economically costly. The nanosized particle's tendency to agglomerate, the difficult recovery from the irradiation media, or the low efficiency under visible light irradiation are several drawbacks that result in the overuse of high amounts of TiO_2 [12,16–23].

To solve most of these problems, supporting materials can be coated with photocatalyst nanoparticles. In this context, core@shell SiO_2@TiO_2 composites have been the most extended materials to prevent nanosized particle agglomeration and improve media recovery [22,23]. A range of

* Corresponding author.
E-mail addresses: marmarin@qim.upv.es (M. Luisa Marin), fbosca@itq.upv.es (F. Bosca).

https://doi.org/10.1016/j.jphotochem.2023.114917
Received 21 April 2023; Received in revised form 2 June 2023; Accepted 5 June 2023
Available online 8 June 2023

core@shell composites has been prepared by modifying morphology, thickness shell, or core size to get improved properties [24]. Moreover, silica has been chosen as a suitable *core* option due to its easy preparation with size control, low cost, and high thermal and mechanical stability [21,23]. Sol-gel and hydrothermal methods are the most extended procedures for TiO_2 coating on silica, but the atomic layer deposition method has also been used [16,18,20–23]. Advantages of the sol–gel synthesis include the homogeneous coverage of TiO_2 on the surface of silica and the possibility of getting a titania shell with different nanoparticle crystal sizes [18]. However, problems associated with this synthesis are related to fast hydrolysis and condensation of titanium alkoxides, which often lead to the agglomeration of particles, as well as the formation of unsupported titania particles via homogeneous nucleation [22,25]. Complexing agents or ammonia have been used to minimize these particles' agglomerations [25]. The hydrothermal method also shows disadvantages, such as non-homogeneous coverages by titania shells with TiO_2 crystal size of only *ca.* 5 nm [23].

Key parameters for the photocatalytic properties of SiO_2@TiO_2 composites include the crystallite size and shape of anatase nanoparticles as well as the thickness of the TiO_2 shell. These properties are directly related to light absorptivity, surface area, and charge carrier dynamics [16,18–23,26–29]. In this sense, several studies investigated the photo-reactivity of SiO_2@TiO_2 composites *versus* the thickness of the TiO_2 shell with inconclusive results. Thus, thickness values between *ca.* 10 nm till *ca.* 50 nm have been proposed to provide the best photoreactivity of SiO_2@TiO_2 composites [16,20–23,30]. In addition, some of them have evidenced that the agglomeration of TiO_2 nanocrystals in a TiO_2 shell has better photocatalytic activity than pure titania nanoparticles [22,23]. In other studies, the different photocatalytic reactivity of the SiO_2@TiO_2 composites has mainly been correlated with the specific surface area (SSA) and the adsorption capabilities of the materials [31–33]. However, the photo-reactivity of these composites has not been evaluated based on the light absorbed as a key factor for understanding the photocatalytic activity of SiO_2@TiO_2. In this sense, changes in the size and crystal phase of TiO_2 nanoparticles are correlated with light harvesting and, therefore, with the efficiency of the photo-excited electron-hole processes [27–29].

Thousands of articles dealing with different aspects of TiO_2 are currently being published [34–37]. Although most of the fundamental processes of TiO_2 photocatalysis have been extensively investigated under well-controlled conditions, the role of surface excess charges, surface additives, or the dependence between the light source irradiance and the optimal amount of TiO_2 to carry out photocatalytic processes still remain unclear. This last aspect can be of fundamental interest to eventually transfer the technology based on supported photocatalysts to real industry, making reasonable use of applied light.

With this background, the aim of this contribution is to determine the most efficient TiO_2 shell thickness in the supported TiO_2 photocatalysts. With this purpose, several SiO_2@TiO_2 composites, with titania nanocrystals of *ca.* 12 nm covering the silica spheres homogeneously, were prepared using a modified sol–gel method for fine control of the crystallinity of TiO_2 and the shell thickness. Then, the SiO_2@TiO_2 heterogeneous materials were submitted for an exhaustive characterization and a careful analysis of their photocatalytic activity. Parameters such as TiO_2 thickness, surface area, and percentage of TiO_2 in each photocatalyst were evaluated against the model pollutant methylene blue.

2. Experimental

2.1. Chemicals

P25 Aeroxide, Isopropanol, methylene blue (MB), tetraethyl orthosilicate (TEOS) 99.0 %, titanium (IV) isopropoxide (TTIP) 99.0 %, and trimethoxybenzoic acid were purchased from Sigma Aldrich. Ammonium hydroxide 28–30 % was purchased from Fischer. The water used in the photodegradation experiments was distilled grade. Acetonitrile (ACN), ethanol of HPLC quality, and acetone were purchased from Scharlab.

2.2. Synthesis of the SiO_2@TiO_2 core@shell photocatalysts (ST composites)

The synthesis of the SiO_2 particles was based on the Stöber method [38]. Briefly, 1 mmol of TEOS was added to 500 mL of EtOH in the presence of 6.5 mmol of NH_4OH under stirring at 0 °C. After 2 h at this temperature, the reaction was conducted at room temperature for 24 h. The particles were centrifuged at 3500 rpm for 10 min and then washed three times with 150 mL of EtOH. The product was stored under vacuum conditions.

Different amounts of TTIP (vide infra) in isopropanol (16 mL) were added dropwise to a mixture of the synthesized SiO_2 particles (2.00 g) suspended in EtOH (80 mL) under stirring. Then, the reaction mixture was heated up to 70 °C. After the first 30 min of reaction, the mixture was submitted to a humidified airflow of 100 mL min^{-1} for 20 h. The resulting suspension was centrifuged at 3500 rpm for 10 min, washed with EtOH and H_2O, dried under vacuum overnight, and milled in an Agatha mortar. The synthesized SiO_2@TiO_2 (ST composites) were calcined at 500 °C for 2 h with a temperature ramp of 10 °C min^{-1}.

Following the above-detailed protocol, ST-14, ST-32, and ST-42 core@shell photocatalysts were synthesized using 1.8, 3.6, and 7.2 mmol TTIP per gram of SiO_2, respectively. A further core@shell photocatalyst (ST-25) was synthesized following the described procedure in which 3.6 mmol TTIP per gram of SiO_2 was used, but the centrifugation speed applied was 10000 rpm for 10 min.

2.3. Adsorption experiments

The adsorption of MB over the heterogeneous surface was evaluated as follows: SiO_2@TiO_2 composite (10 mg each) was added to MB (1×10^{-4} M, 2 mL) and kept under continuous stirring for 1 h and in the absence of light. After that time, an aliquot of 250 μL was subtracted, filtered, and then diluted with 2.75 mL of EtOH. The corresponding absorption spectrum was recorded and compared to the spectrum of a control solution made with 250 μL of MB (1×10^{-4} M) in 2.75 mL of H_2O.

2.4. Photocatalytic degradation reactions

Different amounts of SiO_2@TiO_2 composites and P25 (from 0.5 to 25 mg) were added to cylindrical glass vials of 1.5 cm internal diameter containing 5 mL of MB (1×10^{-4} M). After 1 h of vigorous magnetic stirring in absence of light, the different mixtures were irradiated in a Luzchem Research Inc., using 8 lamps of 8 W (λ_{em} was centered at 352 nm), keeping the magnetic stirring. Samples were placed at *ca.* 10 cm (light intensity was 3.8 mW cm^{-2}). Aliquots of 0.5 mL were taken at different irradiation times, mixed with 0.5 mL of EtOH, and stirred for 10 min under dark conditions to ensure the desorption of every compound from the photocatalyst surfaces. Then, they were filtered, and 400 μL of each sample was diluted with 2.6 mL of EtOH prior to analyzing the MB absorption band at 656 nm in the UV–Vis absorption spectrum registered from 200 to 800 nm. All the experiments were performed in triplicates.

2.5. Photoluminescence emission measurements

Photoluminescence emission spectra on ST-14, ST-32, and ST-42 were performed in an FLS1000 spectrometer (Edinburgh Instruments) using a 450 W Xe lamp as the excitation source. Their emission lifetimes were determined upon excitation with a pulsed laser diode at 366 nm.

2.6. Photocurrent measurements

Chronoamperometry curves were performed using a Gamry Instruments potentiostat. A standard three-electrode configuration was used in a homemade quartz electrochemical cell with a platinum wire as the counter electrode and a saturated Ag/AgCl electrode as the reference. The working electrode was prepared as described below.

Preparation of photocatalyst electrodes (working electrodes): First, a paste of each material was obtained by mixing 50 mg of photocatalyst with 0.5 mL of terpineol and 1 mL of acetone. The mixture was left stirring overnight; then, the cap was opened and left until the acetone completely evaporated. Then, 25 μL of each sample was spread onto a conductive carbon paper with dimensions of approximately 2.0 × 1.0 cm^2. The resulting final area was 1.0 × 1.0 cm^2. Finally, the electrode was sintered at 450 °C for 30 min.

Characterization of the electrodes: The photocurrent generated by the electrodes was measured at 0.4 V for 10 cycles of light on/off, with each cycle having a duration of 20 s. A 0.5 M Na_2SO_4 electrolyte solution was used. Prior to the measurements, the solutions were purged with argon for 10 min. UV–Vis irradiation of the working electrodes was carried out with a spotlight Hamamatzu Xe lamp (Lightnincure LC8 model, 800–200 nm, 1000 W/m^2, fiber optic light guide with a spot size of 0.5 cm).

3. Results and discussion

3.1. Morphology and composition of the synthesized SiO_2@TiO_2 materials

Four SiO_2@TiO_2 composites with different TiO_2 shell thicknesses were prepared using SiO_2 microspheres as supporting substrates: ST-14, ST-25, ST-32, and ST-42. First, an initial synthesis of SiO_2 microparticles (525 + 21 nm, see Figure S1) was made through the Stöber method [38]. Afterward, SiO_2 spheres were covered by amorphous TiO_2 using different amounts of TTIP (see Table 1) in i-propanol:EtOH (0.2:1, 96 mL) as solvent at 70 ^{0}C. In this point, considering that TTIP presents a high reactivity in the presence of H_2O, a continuous humified air flow of 100 mL min^{-1} was applied for 20 h to control the hydrolysis/condensation rate of titania over the SiO_2 spheres. Finally, the synthesized materials were washed with EtOH and H_2O, centrifuged at 3500 rpm or 10000 rpm for 10 min, and calcined at 500 °C for 2 h to give rise to ST-14, ST-25, ST-32, and ST-42 composites.

The average diameter and morphology for the SiO_2@TiO_2 composites were studied from TEM and HRFESEM (see representative images in Fig. 1). The composites display, in all cases, a rough surface (see Fig. 1A–D), in contrast to the smooth spherical shape of the SiO_2 used as a support (see Figure S1). The final diameters for the synthesized composites are shown in Fig. 1E–H and Table 1. In this sense, composites ST-14, ST-32, and ST-42 showed TiO_2 shell thicknesses of *ca.* 14, 32, and 42 nm, respectively. It is interesting to mention that increasing the speed of the centrifugation step in the process of synthesizing composite ST-32 from 3,500 rpm to 10,000 rpm resulted in a narrower TiO_2 shell (see ST-32 *versus* ST-25). In fact, after the subsequent calcination process, the TiO_2 shell in ST-25 displays a thickness of *ca.* 25 nm. In a more careful analysis of the surface for the synthesized composites by HRFESEM (Fig. 1I–L), it can be observed that the TiO_2 shell has been generated over all the SiO_2 surfaces, resulting in a homogeneous TiO_2 nanocrystalline shell. Finally, an EDS mapping of each photocatalyst supports the homogeneous distribution of the TiO_2 over the SiO_2 spheres (see Fig. 1M–P and Figures S2-S3). This result also demonstrates that the incorporation of a continuous humidified airflow in the sol–gel TiO_2 synthesis allows control over the creation of a homogeneous shell on the silica surface.

HRTEM provides further support for the crystalline nature of the shell (see Fig. 2 and Supporting Information Section 4). Hence, Fig. 2A–B show a continuous uniform distribution of closely attached TiO_2 nanocrystals in the TiO_2 shell for the ST-32 composite, which was supported by the outcomings provided by the dark field HRTEM image (Fig. 2C) [39]. Moreover, interplanar distances of 0.374 nm, 0.259 nm, and 0.219 nm were determined from the selected area electron diffraction (SAED) pattern of the ST-32 titania shell (Fig. 2D). These values correspond to (1 0 1), (1 0 3), and (0 0 4) crystal planes of pure anatase (JCPDS# 21-1272) [40].

X-ray diffraction (XRD) patterns and Raman spectroscopy also provided evidence of the anatase crystalline phase of the TiO_2 shell on the SiO_2-TiO_2 spheres. Diffractograms obtained from ST-14, ST-25, ST-32, and ST-42 photocatalysts display a broad band centered at 2θ = 22° attributable to the presence of the amorphous SiO_2 cores (Fig. 3A). Additionally, each diffractogram shows the representative 2θ = 25°, 38°, 48°, 55°, and 63°, which are associated to the pure TiO_2 anatase crystal phase. This confirms the selective crystallization into the photoactive TiO_2 anatase phase upon calcination at 500 °C (JCPDS# 21-1272) [41]. This fact could be promoted by the SiO_2 since it could inhibit the transformation phase of anatase to rutile [42]. It must be noted that the Full Width at Half Maximum (FWHM) for the TiO_2 on the composites was reduced compared to the SiO_2 particles. SiO_2 particles are constituted by an amorphous atomic matrix which is translated into a broad peak in XRD spectra [43]. In this sense, amorphous components

Table 1
Summary of experimental conditions used in the synthesis of SiO_2@TiO_2 photocatalysts (composites) and their different (photo)physicochemical properties.

Composites	TTIP[a] (mmol / g of SiO_2)	Centrifugation[b] (rpm)	Particle diameter[c] (nm)	Content of TiO_2[d] (%, w/w) ICP	Content of TiO_2[e] (%, w/w) EDS	A_{BET}[f] (m^2 / g)	ζ-potential (mV)	k_R[g] (min^{-1})
ST-14	1.8	3,500	553 ± 26 (*ca.* 14)[h]	7.6	7.4	32.3	-21.65	0.08 ± 0.01
ST-25	3.6	10,000	575 ± 22 (*ca.* 25)[h]	12.2	16.6	25.1	-19.90	0.09 ± 0.01
ST-32	3.6	3,500	590 ± 23 (*ca.* 32)[h]	14.7	21.6	20.1	-19.52	0.12 ± 0.01
ST-42	7.2	3,500	609 ± 28 (*ca.* 42)[h]	21.7	28.1	27.6	-11.73	0.07 ± 0.01

[a] Amount of TTIP (mmol/g of SiO_2).
[b] centrifugation speed (rpm).
[c] particle diameter (nm) obtained from TEM.
[d] content of TiO_2 (in % w/w) determined by ICP.
[e] content of TiO_2 (in % w/w) determined by EDS.
[f] area (m^2 g^{-1}) determined by the BET method.
[g] MB maximum photodegradation rate constant at the fixed photon fluxed: k_R (min^{-1}).
[h] TiO_2 shell thickness of a photocatalyst particle, which is obtained from equation: shell thickness = (SiO_2@TiO_2 diameter - SiO_2 diameter)/2. The experimentally determined SiO_2 diameter is 525 ± 21 nm (see SI).

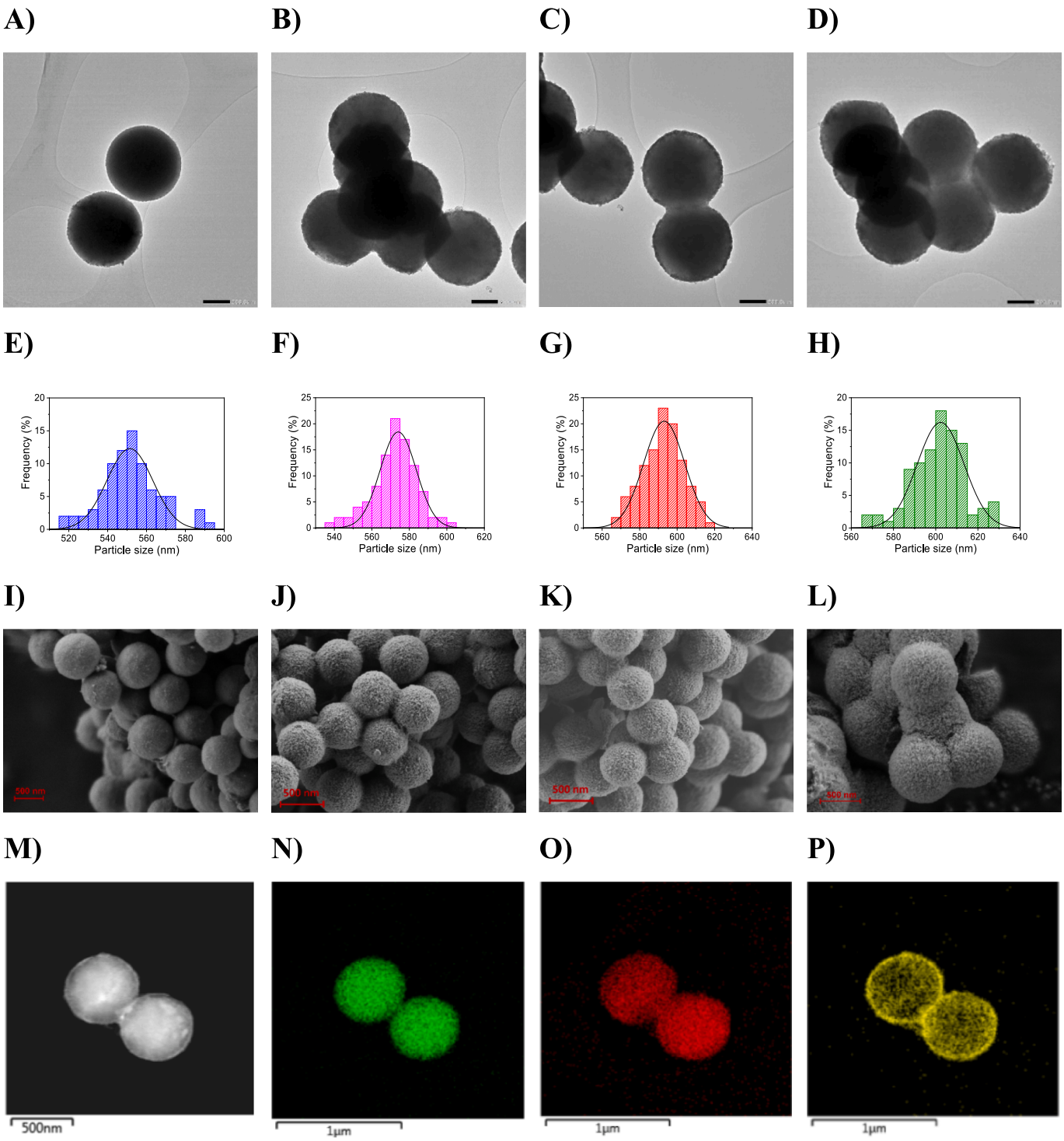

Fig. 1. (A – D) TEM, (E – H) particle distribution, and (I – L) HRFESEM images for ST-14, ST-25, ST-32, and ST-42 photocatalysts, respectively. (M) STEM image, and (N) Si, (O) O, and (P) Ti elemental mapping by EDS analysis for ST-32 photocatalyst.

display a lack of long-range crystallographic order, as they do not produce diffraction patterns. It is worth noting that XRD patterns for amorphous phases can appear similar to those observed for nanoparticles with diameters less than 2 nm; both would exhibit similar, significant peak broadening [44]. Additionally, crystalline products, such as the TiO_2 shell on our SiO_2@TiO_2 photocatalysts, display a high signal-to-noise ratio and sharp peaks [44], which will explain that the FWHM of the ST-25, ST-32, and ST-42 are reduced compared to the SiO_2 particles.

Furthermore, the anatase crystallite size was determined from the FWHM of the $2\theta = 25°$ peak through the Scherrer equation ($D = k \times \lambda / FWHM \times Cos(\theta)$), where D is the crystallite size, $\boldsymbol{k}$ represents the Scherrer constant value, ranging from 0.62 to 2.08, depending on the diffraction and crystal shape [45], λ is the wavelength of the X-Ray and $\boldsymbol{\theta}$ is the diffraction angle in radians [46,47]. The crystal size for the synthesized photocatalysts was averaged at *ca.* 12 nm, which agrees with the TiO_2 crystal size described in the literature for calcinations at 500 °C of other SiO_2@TiO_2 composites [18]. Furthermore, the Raman spectra of

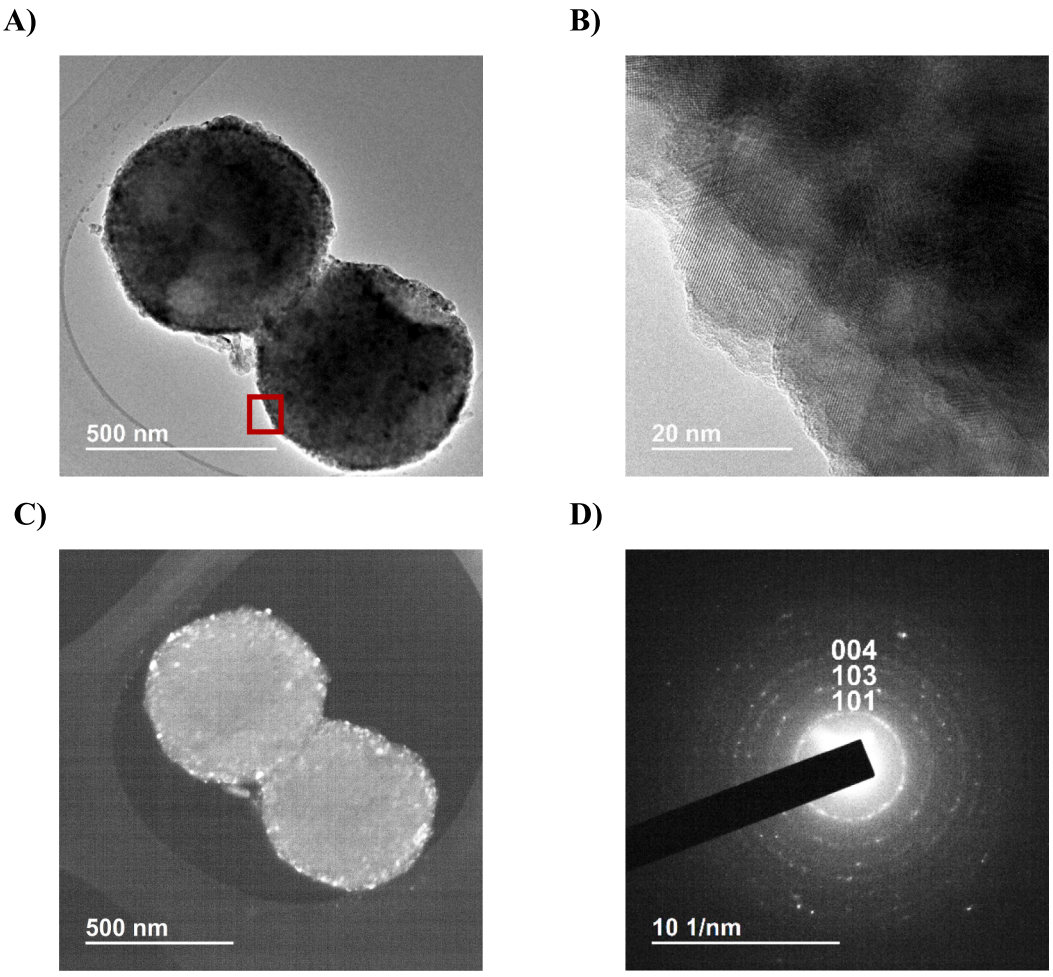

Fig. 2. (A) HRTEM bright field representative image of ST-32 composite. (B) Detailed image of the crystalline structure of the TiO_2 shell, (C) HRTEM dark field image of ST-32, and (D) SAED pattern of the TiO_2 anatase shell.

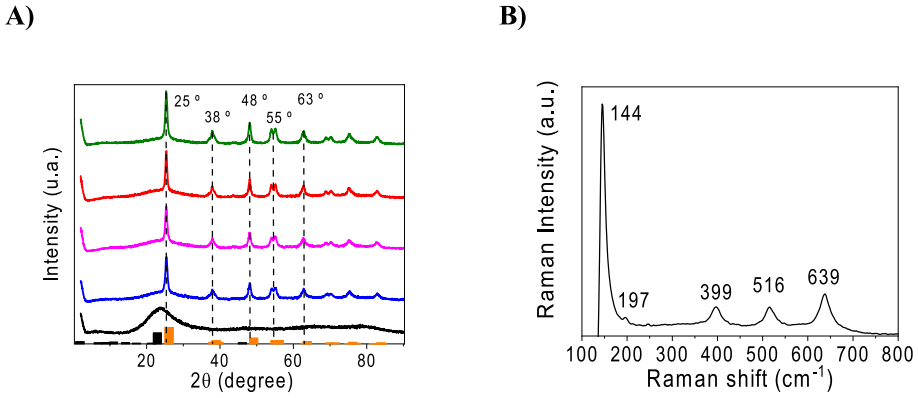

Fig. 3. (A) From top to down, powder X-ray diffractograms for ST-42 (green), ST-32 (red), ST-25 (pink), ST-14 (blue), and SiO_2 particles (black). Black and orange bars represent the theoretical signals for amorphous SiO_2 (JCPDS# 46-1045) and TiO_2 anatase phase (JCPDS# 21-1272), respectively. (B) Representative Raman spectrum of the ST-32 photocatalyst.

all the photocatalysts showed the reported typical signals of the anatase TiO_2 phase: E_g (143 cm^{-1}), E_g (195 cm^{-1}), B_{1g} (394 cm^{-1}), A_{1g} (514 cm^{-1}), E_g (636 cm^{-1}) (see Fig. 3B for ST-32, and Figure S5 for ST-14, ST-25, and ST-42) [48].

The content of TiO_2 for the synthesized photocatalysts (% w/w) was determined by ICP and STEM-EDS (see Table 1). Specifically, the percentage of TiO_2 from ICP in ST-14, ST-25, ST-32, and ST-42 was 7.6 %, 12.2 %, 14.7 %, and 21.7 %, respectively, which are in accordance with the different thicknesses of the TiO_2 shell. On the other hand, from the STEM-EDS analysis, slightly different values for the TiO_2 content were found: 7.4 %, 16.6 %, 21.6 %, and 28.1 % for ST-14, ST-25, ST-32, and ST-42, respectively. Although differences between ICP and STEM-EDS can be related to the accuracy of each technique, the found TiO_2 % (w/w) content is directly correlated to the TiO_2 thickness displayed by the shell in each composite.

3.2. Surface properties of SiO_2@TiO_2 composites

The specific surface area (SSA) of a photocatalyst is one of the key parameters to be considered when analyzing the interfacial properties and the photocatalytic activity. Hence, nitrogen physisorption analyses were carried out with the synthesized photocatalysts to determine their SSA and to study their pore structure using the Brunaer-Emett-Teller (BET) method [49]. Fig. 4A shows type IV nitrogen adsorption–desorption isotherms and type III hysteresis for all the SiO_2@TiO_2 photocatalysts. These kinds of isotherms are characteristic of solids consisting of aggregates or agglomerated crystals [50]. From them, SSA values in the same order of magnitude, ranging from 32.3 m^2 g^{-1} for ST-14 to 20.1 m^2 g^{-1} for ST-32, were determined (see Table 1). Porous measurements follow the same tendency displayed by SSA. In this sense, the porous size decreases with the increase in the shell thickness. Probably, higher amounts of TiO_2 imply a smaller separation between crystals which entails that the porous size decreases (Figure S6). In the case of ST-42, the higher thickness resulted in a slightly higher SSA value than expected. Perhaps, the most external TiO_2 nanocrystal layer on the ST-42 shell is less compact than the internal layers, leading to cavities between TiO_2 crystals with greater sizes and volumes than those in the more internal layers.

Adsorption capacity and surface charge are usually correlated and play an important role in eliminating organic pollutants in water media. Thus, the absorption capacity of the synthesized photocatalysts was evaluated using MB as a representative model organic contaminant. As is shown in Fig. 4B, some differences can be observed. In this sense, adsorption of 68 %, 58 %, 60 %, and 54 % were determined for the ST-14, ST-25, ST-32, and ST-42, respectively. Moreover, the results obtained for ζ-potential measurements recorded in an aqueous solution of pH *ca.* 7.0 were −21.65 mV, −19.90 mV, −19.52 mV, and −11.73 mV for the ST-14, ST-25, ST-32, and ST-42, respectively. Interestingly, the ζ-potential value for TiO_2 photocatalysts becomes less negative as the TiO_2 shell thickness increases. This fact can be understood by considering that the ζ-potential for SiO_2 spheres is *ca.* −40 mV, while that reported for TiO_2 nanoparticles (P25) is *ca.* −10 mV [51,52]. Thus, the experimentally recorded values indicate that the nanocrystal TiO_2 shell around the SiO_2 spheres could leave partial access to the silica surface through the porous framework, but this accessibility decreases as the TiO_2 shell thickness get bigger.

A good correlation is found between the MB adsorption and the surface charge of all the photocatalysts. However, this trend does not correlate well with the values of SSA found for the composites. For instance, the highest adsorption percentage observed for ST-14 is governed by its highest SSA and also agrees with its ζ-potential, which may enhance the adsorption capacity of the cationic MB. However, ST-42 shows the smallest MB adsorption despite its SSA is not the smallest one of the synthesized photocatalysts. Probably, its less negative ζ-potential value balances its great SSA, giving rise to lower adsorption than that shown by the other composites.

3.3. Band gap determination for SiO_2@TiO_2 composites.

Diffuse reflectance spectroscopy was recorded to determine the semiconductor optical band gap, which defines the photocatalyst activation wavelength. Results were expressed as the Kubelka-Munk function using the Tauc plot method (Fig. 5) [53]. The experimental UV–Vis spectra for the SiO_2@TiO_2 composites display an increase in light absorption and a red shift as the shell thickness increases, which can be associated with the Rayleigh scattering produced by TiO_2 nanocrystals, as previously reported [23]. The determined band gap values were 3.25 eV, 3.35 eV, 3.34 eV, and 3.31 eV for the ST-14, ST-25, ST-32, and ST-42 photocatalysts, respectively.

3.4. Photocatalytic activity of the SiO_2@TiO_2 composites

The photo-reactivity of the composites *versus* the light absorbed was evaluated in the degradation of the model pollutant Methylene Blue (MB, 1×10^{-4} M) in aqueous aerobic media. For that purpose, a light source with an emission centered at λ_{em} = 352 nm and a fixed light intensity of 3.8 mW/cm^2 was employed, while the concentration of each photocatalyst varied from 0.25 to 5 mg mL^{-1}. Commercial P25 (crystallite sizes of *ca.* 21 nm and SSA of *ca.* 55 m^2/g) was also tested with the aim of comparing the photocatalytic efficiency displayed by the

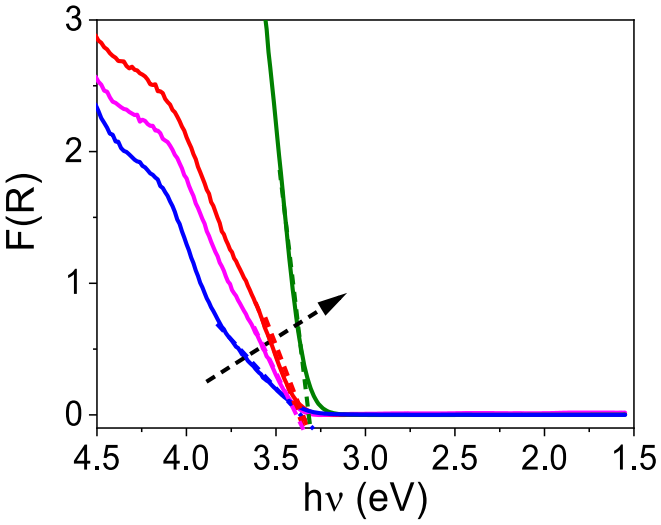

Fig. 5. Kubelka-Munk transformed diffuse reflectance spectra for ST-14 (blue), ST-25 (pink), ST-32 (red), and ST-42 (green). Dashed lines denote the linear tendencies that define the optical band gap for each composite.

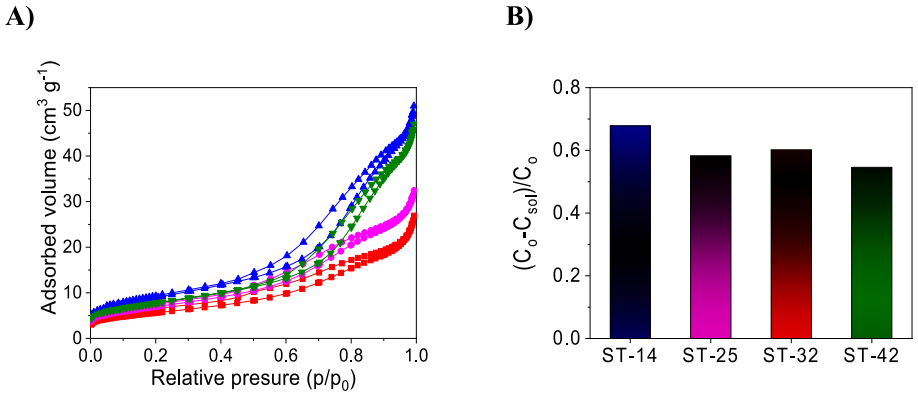

Fig. 4. N_2 adsorption–desorption isotherms (A) and relative MB adsorption (B) for ST-14 (blue), ST-25 (pink), ST-32 (red), and ST-42 (green).

unsupported crystalline TiO_2 standard (see Figures 6 and S7).

Fig. 6A shows that in all cases, the photodegradation rate increased with the concentration of the photocatalyst until it reached a plateau. Interestingly, the photocatalytic performance of each photocatalyst at its corresponding plateau increased along with the thickness of the TiO_2 shell up to *ca.* 30 nm. However, a further thickness increment for the TiO_2 shell (ST-42) resulted in a less efficient composite. Moreover, composite ST-42 resulted in being most photoactive than ST-14 till 2 mg mL^{-1} of photocatalyst, but this property is inverted when the amount of photocatalyst is optimized to use all the irradiance. Thus, considering that characterization properties (crystallinity, crystal size, morphology, SSA, band gap, ζ-potential, and adsorption) are quite similar for all the SiO_2@TiO_2 composites, and the same number of photons (light intensity) has been applied, only the relationship between the TiO_2 thickness shell and the efficiency of the photogenerated e^--h^+ pairs could lead to the different photoactivity displayed. Thus, the observed results can be explained by a combination of the agglomeration of TiO_2 nanocrystals in the shell of supported materials [22,23], together with an inefficient photoreactivity of the inaccessible surface of the shell.

Hence, the increasing photocatalytic activity of SiO_2@TiO_2 composites from ST-14 to ST-32 can mainly be attributed to the growth of the number of TiO_2 nanocrystals in the shell. Probably, the partial associations of TiO_2 crystallites with sizes close to 12 nm reduce the e^--h^+ recombination process. However, in the case of ST-42, this effect is overcome by the increase of the inaccessible surface of the TiO_2 shell. Only when more light than needed is applied, is ST-42 a better photocatalyst than ST-14 because ST-42 has many more TiO_2 nanocrystals than ST-14 and consequently generates a higher number of accessible e^--h^+ pairs. Nonetheless, when all the applied light is absorbed by both photocatalysts, ST-14 is more photoactive because although the photogenerated e^--h^+ pairs would be the same for both composites, the number of accessible e^--h^+ pair events would be higher for ST-14.

A representation of the reactivity of photocatalysts vs TiO_2 content (see Fig. 6B) shows the same trend. In this case, it can be clearly observed that the agglomeration of TiO_2 nanocrystals in the shell of supported materials produces a relevant positive effect only for ST-32, while for ST-42, this high nanocrystal agglomeration turns negative because it produces an important increase of inaccessible surface of TiO_2.

Moreover, Fig. 6B shows that all the light is absorbed at a TiO_2 content of *ca.* 0.6 mg mL^{-1} for all photocatalysts, including P25 (see also Fig. 6A). This study was performed using P25 as a reference photocatalyst, and P25 resulted in being the most efficient photocatalyst when efficiencies were compared both by concentration and by the content of TiO_2. This behavior could be attributed to its high SSA and to its specific crystallinity because the presence of rutile also decreases the e^--h^+ recombination process, and probably, all e^--h^+ pair events are accessible.[54] Nevertheless, ST-32 only showed a photoreactivity 1/3 lower than the one found for P25. Even more important, it has been demonstrated that a shell thickness of *ca.* 30 nm is optimum to prepare highly efficient supported photocatalysts based on TiO_2.

3.5. Photoluminescence and photoelectric studies

The photophysical behavior of ST-14, ST-32, and ST-42 photocatalysts was analyzed through photoluminescence (PL). It is commonly accepted that emission, lifetime, and quantum yield are significant measurements that strongly depend on many factors, such as crystal structure, particle size, and optical configuration [55].

Many researchers have correlated TiO_2 PL intensity with the charge carriers (e^--h^+) recombination performance and, therefore, with photocatalytic activity [56–58]. Although it is generally accepted that oxygen-ion vacancies (O_V) and structural defects play an important role in mediating interfacial electron transfer, their effect on the charge separation process is still under debate [59,60]. Some researchers hold the opinion that O_V act as the recombination centers for the photoinduced electrons and holes [61,62]. However, some others support that the presence of O_V and structural defects would facilitate the charge separation process and, therefore, may improve the photocatalytic activity of composites [63,64].

Fig. 7 shows the PL spectra for the ST-14, ST-32, and ST-42 composites. They all exhibited a broad band at 430 nm generated by a self-trapped exciton (STE) [65–67]. Since all the composites were synthesized under similar conditions, PL intensity variation could be attributed to the changes in the O_V and to the structural defects' concentration on the different TiO_2 shells [68]. In this way, the low emission intensity displayed by ST-32 could be translated into a low recombination efficiency for the e^--h^+ charge carriers, probably due to the presence of a higher concentration of shallow defect states, which would be acting as e^--h^+ trappers [69]. In addition, the presence of shallow defects often couples with the introduction of other components (such as Ti^{3+}), which are also found to largely affect the charge separation process [70]. On the other hand, the high emission intensity displayed by the ST-14 photocatalyst results from more efficient recombination of the photoinduced e^--h^+ [71]. Moreover, the agglomerate nature of the wide TiO_2 shell in ST-42 may lead to the formation of bulk defect states throughout the semiconductor structure, which behaves as charge carriers where the e^--h^+ also recombines [72].

Overall, our results are more closely related to those authors who support the lack of e^--h^+ recombination through the electron transfer

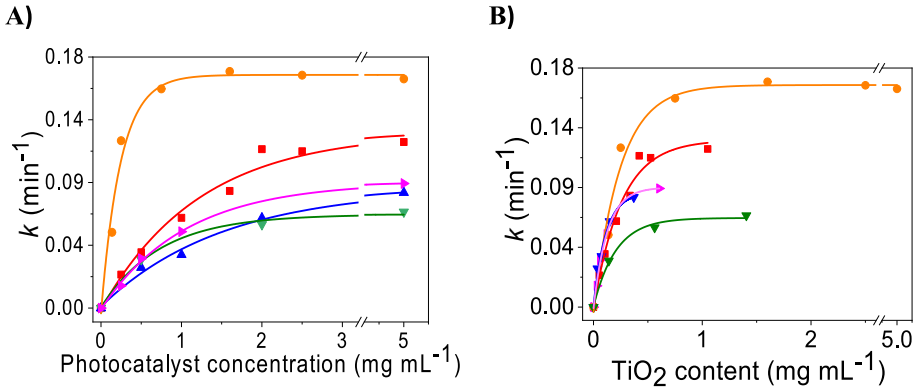

Fig. 6. Photodegradation rate constants of MB (1×10^{-4} M) in aerated aqueous mixtures *versus* photocatalyst concentration (A) and *versus* TiO_2 content (B): ST-14 (▲), ST-25 (▶), ST-32 (■), ST-42 (▼), and P25 (●). Irradiations were performed with 8 lamps (λ_{max} = 352 nm) at a fixed light intensity of 3.8 mW/cm^2.

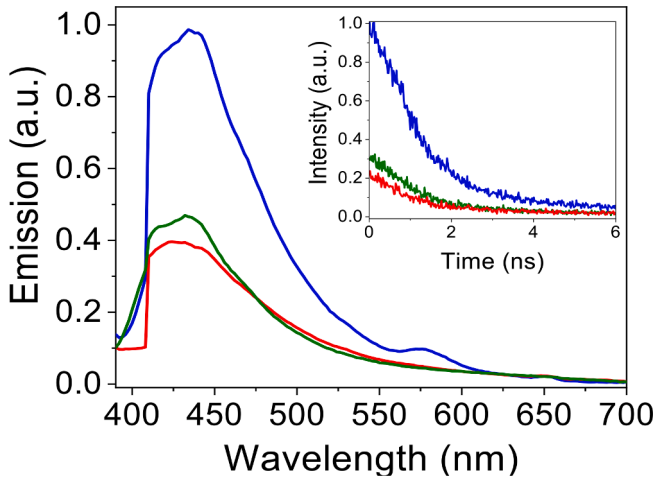

Fig. 7. Photoluminescence spectra and time-resolved emission (inset) of ST-14 (blue), ST-32 (red), and ST-42 (green) photocatalysts. Samples were measured as solid dispersions in a quartz cuvette at λ_{exc} = 366 nm.

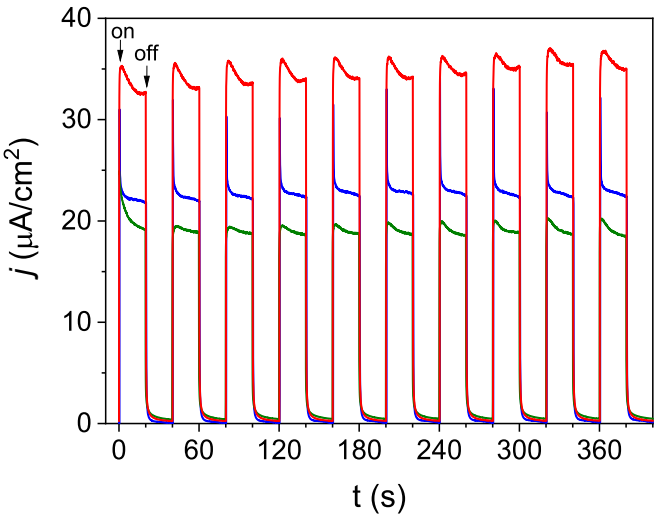

Fig. 8. Photocurrent density-time curves with 20 s on/off cycles of ST-14 (blue), ST-32 (red), and ST-42 (green).

process from the TiO_2 conduction band to O_V and structural defects. In fact, this effect could be responsible for the different photocatalytic efficiencies observed for the different photocatalysts. Thus, ST-32 presents the most photocatalytic efficient TiO_2 thickness shell found in this study, and probably, this behavior is promoted by the major concentration of O_V and structural defects in its shell, as PL studies revealed. They could act as electron acceptors, trapping the photogenerated electrons temporarily to reduce the surface recombination of e^--h^+ pairs. As the redox reactions might occur on the surface of O_v, the O_V and structural defects can be considered the active sites of the TiO_2 photocatalyst [73,74]. In this sense, Shekiya *et al.* observed TiO_2 emission at 413 nm and attributed this peak to an oxygen vacancy located at 3.0 eV with two trapped electrons [75]. Hence, the proper ionization energy of the O_v leads to favorable O_2 reduction, favoring the photocatalytic cycle and avoiding the e^--h^+ recombination.

Furthermore, the lowest emission lifetime value recorded for ST-32, which is 0.66 ns (see inset of Fig. 7), is due to the highest abundance of O_v and structural defects. On the contrary, higher values were found for ST-14 and ST-42 (0.77 and 0.81 ns, respectively) in agreement with the lower abundance of O_v and structural defects and with bulk defects, respectively.

To give further evidence to support the photocatalytic activity studied, the photocurrent response of the materials was evaluated. Fig. 8 shows the chronoamperometry curves of the three prepared photocatalyst electrodes. The ST-32 electrode shows the highest photogenerated current, while the ST-14 electrode generates slightly more current than the ST-42 electrode. Considering that a higher photocurrent is associated with a more efficient separation of photoinduced electron-hole pairs, these results agree with the studied photocatalytic activity and support the idea that controlling the shell length of TiO_2 over SiO_2 spheres is crucial for optimizing the photocatalytic activity.

4. Conclusions

Several SiO_2@TiO_2 composites with different robust and homogeneous TiO_2 shell thicknesses were synthesized by applying a modification of the sol–gel method. The high control that the synthetic method brings over the modulation of the TiO_2 shell thickness enables the formation of different SiO_2@TiO_2 photocatalysts to study the raised hypothesis about the dependence between the TiO_2 shell thickness, light harvesting, and photocatalytic efficiency. The photocatalytic tests performed using methylene blue and a fixed intensity of UVA light revealed that the optimum TiO_2 shell thickness is *ca.* 30 nm. Higher thickness values decrease the photodegradation efficiencies because many photo-excited electron-hole pair events will occur in inaccessible locations of the TiO_2 shell. Emission studies and the photocurrent response of the materials also agreed with the photocatalytic results. Moreover, the results of this photocatalytic study have shown the relevance of using the optimum concentration of each photocatalyst not to waste light. Finally, it is noteworthy that these findings have revealed the importance of designing and synthesizing robust heterogeneous photocatalysts with a shell thickness in accordance with the light irradiance. These findings open opportunities for developing of novel robust SiO_2@TiO_2 supported photocatalysts.

CRediT authorship contribution statement

Oscar Cabezuelo: Investigation, Writing – original draft. **Ander Diego-Lopez:** Investigation. **Pedro Atienzar:** Investigation, Methodology, Validation. **M. Luisa Marin:** Conceptualization, Funding acquisition, Project administration, Supervision, Validation, Writing – review & editing. **Francisco Bosca:** Conceptualization, Funding acquisition, Project administration, Supervision, Validation, Writing – review & editing.

Declaration of Competing Interest

The authors declare that they have no known competing financial interests or personal relationships that could have appeared to influence the work reported in this paper.

Data availability

Data will be made available on request.

Acknowledgments

The authors would like to acknowledge the Spanish Ministry of Science, Innovation, and Universities (PID2019-110441RB-C33 financed by MCIN/AEI/10.13039/501100011033 and TED2021-131952B-I00 financed by MCIN/AEI /10.13039/501100011033 and by European Union NextGenerationEU/PRTR). O. Cabezuelo and A. Diego-Lopez are indebted to the Universitat Politècnica de València for the corresponding Predoctoral FPI fellowship (FPI-UPV/Subprograma 1). The authors would like to acknowledge the Servei de Microscopia Electrònica from the Universitat Politècnica de València (UPV) for the support on the composite characterization and sample preparation.

Funding for the open access charge provided by CRUE-Universitat Politècnica de València is acknowledged.

Appendix A. Supplementary material

Supplementary data to this article can be found online at https://doi.org/10.1016/j.jphotochem.2023.114917.

References

[1] A.V. Suhogusoff, R. Hirata, L.C.K.M. Ferrari, Water quality and risk assessment of dug wells: A case study for a poor community in the city of São Paulo, Brazil, Environ, Earth Sci. 68 (2013) 899–910, https://doi.org/10.1007/s12665-012-1971-x.

[2] M. Jiménez-Totozintle, I. Oller, A. Hernández-Ramírez, S. Malato, M. I. Maldonado, Remediation of agro-food industry effluents by biotreatment combined with supported TiO2/H2O2 solar photocatalysis, Chem. Eng. J. 273 (2015) 205–213, https://doi.org/10.1016/j.cej.2015.03.060.

[3] O. Botalova, J. Schwarzbauer, T. Frauenrath, L. Dsikowitzky, Identification and chemical characterization of specific organic constituents of petrochemical effluents, Water Res. 43 (2009) 3797–3812, https://doi.org/10.1016/j.watres.2009.06.006.

[4] E.M. Saggioro, A.S. Oliveira, T. Pavesi, M.J. Totozintle, M.I. Maldonado, F. V. Correia, J.C. Moreira, Solar CPC pilot plant photocatalytic degradation of bisphenol A in waters and wastewaters using suspended and supported-TiO2. Influence of photogenerated species, Environ. Sci. Pollut. Res. (2014) 12112–12121, https://doi.org/10.1007/s11356-014-2723-0.

[5] S. Malato, P. Fernández-Ibáñez, M.I. Maldonado, J. Blanco, W. Gernjak, Decontamination and disinfection of water by solar photocatalysis: Recent overview and trends, Catal. Today. 147 (2009) 1–59, https://doi.org/10.1016/j.cattod.2009.06.018.

[6] T. Wintgens, F. Salehi, R. Hochstrat, T. Melin, Emerging contaminants and treatment options in water recycling for indirect potable use, Water Sci. Technol. 57 (2008) 99–107, https://doi.org/10.2166/wst.2008.799.

[7] J.-M. Herrmann, Heterogeneous photocatalysis: fundamentals and applications to the removal of various types of aqueous pollutants, Catal Today. 53 (1999) 115–129, https://doi.org/10.1115/IMECE200743738.

[8] H. Gerischer, The impact of semiconductors on the concepts of electrochemistry, Electrochim Acta. 35 (1990) 1677–1699, https://doi.org/10.1016/0013-4686(90)87067-C.

[9] S. Malato, J. Blanco, A. Vidal, C. Richter, Photocatalysis with solar energy at a pilot-plant scale: An overview, Appl. Catal. B. 37 (2002) 1–15, https://doi.org/10.1016/S0926-3373(01)00315-0.

[10] S. Malato, J. Blanco, A. Campos, J. Cáceres, C. Guillard, J.M. Herrmann, A. R. Fernández-Alba, Effect of operating parameters on the testing of new industrial titania catalysts at solar pilot plant scale, Appl. Catal. B. 42 (2003) 349–357, https://doi.org/10.1016/S0926-3373(02)00270-9.

[11] A. Zapata, T. Velegraki, J.A. Sánchez-Pérez, D. Mantzavinos, M.I. Maldonado, S. Malato, Solar photo-Fenton treatment of pesticides in water: Effect of iron concentration on degradation and assessment of ecotoxicity and biodegradability, Appl. Catal. B. 88 (2009) 448–454, https://doi.org/10.1016/j.apcatb.2008.10.024.

[12] J. Carbajo, A. Tolosana-Moranchel, J.A. Casas, M. Faraldos, A. Bahamonde, Analysis of photoefficiency in TiO2 aqueous suspensions: Effect of titania hydrodynamic particle size and catalyst loading on their optical properties, Appl. Catal. B. 221 (2018) 1–8, https://doi.org/10.1016/j.apcatb.2017.08.032.

[13] A. Fujishima, T.N. Rao, D.A. Tryk, Titanium dioxide photocatalysis, J. Photochem. Photobiol. C: Photochem. Rev. (2000) 1–21, https://doi.org/10.1016/S1389-5567(00)00002-2.

[14] N. Serpone, G. Sauvé, R. Koch, H. Tahiri, P. Pichat, P. Piccinini, E. Pelizzetti, H. Hidaka, Standardization protocol of process efficiencies and activation parameters in heterogeneous photocatalysis: Relative photonic efficiencies ζr, J. Photochem. Photobiol. A Chem. 94 (1996) 191–203, https://doi.org/10.1016/1010-6030(95)04223-7.

[15] J. Schneider, M. Matsuoka, M. Takeuchi, J. Zhang, Y. Horiuchi, M. Anpo, D. W. Bahnemann, Understanding TiO2photocatalysis: Mechanisms and materials, Chem Rev. 114 (2014) 9919–9986, https://doi.org/10.1021/cr5001892.

[16] M. Ye, Q. Zhang, Y. Hu, J. Ge, Z. Lu, L. He, Z. Chen, Y. Yin, Magnetically recoverable core-shell nanocomposites with enhanced photocatalytic activity, Chem. A Eur. J. 16 (2010) 6243–6250, https://doi.org/10.1002/chem.200903516.

[17] N. Mandzy, E. Grulke, T. Druffel, Breakage of TiO2 agglomerates in electrostatically stabilized aqueous dispersions, Powder Technol. 160 (2005) 121–126, https://doi.org/10.1016/j.powtec.2005.08.020.

[18] A. Li, Y. Jin, D. Muggli, D.T. Pierce, H. Aranwela, G.K. Marasinghe, T. Knutson, G. Brockman, J.X. Zhao, Nanoscale effects of silica particle supports on the formation and properties of TiO2 nanocatalysts, Nanoscale 5 (2013) 5854–5862, https://doi.org/10.1039/c3nr01287e.

[19] E.P. Ferreira-Neto, S. Ullah, V.P. Martinez, J.M.S.C. Yabarrena, M.B. Simões, A. P. Perissinotto, H. Wender, F.S. De Vicente, P.L.M. Noeske, S.J.L. Ribeiro, U. P. Rodrigues-Filho, Thermally stable SiO2@TiO2core@shell nanoparticles for application in photocatalytic self-cleaning ceramic tiles, Mater Adv. 2 (2021) 2085–2096, https://doi.org/10.1039/d0ma00785d.

[20] P.A. Williams, C.P. Ireland, P.J. King, P.A. Chater, P. Boldrin, R.G. Palgrave, J. B. Claridge, J.R. Darwent, P.R. Chalker, M.J. Rosseinsky, Atomic layer deposition of anatase TiO2 coating on silica particles: Growth, characterization and evaluation as photocatalysts for methyl orange degradation and hydrogen production, J. Mater. Chem. 22 (2012) 20203–20209, https://doi.org/10.1039/c2jm33446a.

[21] F. Wang, L. Feng, Y. Qin, T. Zhao, H. Luo, J. Zhu, Dual functional SiO2@TiO2 photonic crystals for dazzling structural colors and enhanced photocatalytic activity, J. Mater. Chem. C Mater. 7 (2019) 11972–11983, https://doi.org/10.1039/c9tc03426a.

[22] E.P. Ferreira-Neto, S. Ullah, M.B. Simões, A.P. Perissinotto, F.S. de Vicente, P.-L.-M. Noeske, S.J.L. Ribeiro, U.P. Rodrigues-Filho, Solvent-controlled deposition of titania on silica spheres for the preparation of SiO2@TiO2 core@shell nanoparticles with enhanced photocatalytic activity, Colloids Surf. A Physicochem. Eng. Asp. 570 (2019) 293–305, https://doi.org/10.1016/j.colsurfa.2019.03.036.

[23] S. Ullah, E.P. Ferreira-Neto, A.A. Pasa, C.C.J. Alcântara, J.J.S. Acuña, S.A. Bilmes, M.L. Martínez Ricci, R. Landers, T.Z. Fermino, U.P. Rodrigues-Filho, Enhanced photocatalytic properties of core@shell SiO2@TiO2 nanoparticles, Appl. Catal. B. 179 (2015) 333–343, https://doi.org/10.1016/j.apcatb.2015.05.036.

[24] S. Wei, Q. Wang, J. Zhu, L. Sun, H. Lin, Z. Guo, Multifunctional composite core-shell nanoparticles, Nanoscale 3 (2011) 4474–4502, https://doi.org/10.1039/c1nr11000d.

[25] W. Li, J. Yang, Z. Wu, J. Wang, B. Li, S. Feng, Y. Deng, F. Zhang, D. Zhao, A versatile kinetics-controlled coating method to construct uniform porous TiO 2 shells for multifunctional core-shell structures, J. Am. Chem. Soc. 134 (2012) 11864–11867, https://doi.org/10.1021/ja3037146.

[26] F. Dufour, S. Pigeot-Remy, O. Durupthy, S. Cassaignon, V. Ruaux, S. Torelli, L. Mariey, F. Maugé, C. Chanéac, Morphological control of TiO2 anatase nanoparticles: What is the good surface property to obtain efficient photocatalysts? Appl. Catal. B. 174–175 (2015) 350–360, https://doi.org/10.1016/j.apcatb.2015.03.013.

[27] X. Wang, L. Sø, R. Su, S. Wendt, P. Hald, A. Mamakhel, C. Yang, Y. Huang, B. B. Iversen, F. Besenbacher, The influence of crystallite size and crystallinity of anatase nanoparticles on the photo-degradation of phenol, J. Catal. 310 (2014) 100–108, https://doi.org/10.1016/j.jcat.2013.04.022.

[28] C.B. Almquist, P. Biswas, Role of synthesis method and particle size of nanostructured TiO2 on its photoactivity, J. Catal. 212 (2002) 145–156, https://doi.org/10.1006/jcat.2002.3783.

[29] M. Inagaki, R. Nonaka, B. Tryba, A.W. Morawski, Dependence of photocatalytic activity of anatase powders on their crystallinity, Chemosphere 64 (2006) 437–445, https://doi.org/10.1016/j.chemosphere.2005.11.052.

[30] S. Amouzad, N. Monadi, Sensitization of magnetite@SiO2@TiO2 by cobalt sulfophthalocyanine and investigation of photocatalytic activity of oxygen evolution under visible light, Inorg. Chem. Commun. 149 (2023), https://doi.org/10.1016/j.inoche.2023.110401.

[31] K. Urkasame, S. Yoshida, T. Takanohashi, S. Iwamura, I. Ogino, S.R. Mukai, Development of TiO2-SiO2 photocatalysts having a microhoneycomb structure by the ice templating method, ACS Omega 3 (2018) 14274–14279, https://doi.org/10.1021/acsomega.8b01880.

[32] A. Carretero-Genevrier, C. Boissiere, L. Nicole, D. Grosso, Distance dependence of the photocatalytic efficiency of TiO 2 revealed by in situ ellipsometry, J Am Chem Soc. 134 (2012) 10761–10764, https://doi.org/10.1021/ja303170h.

[33] Z.Y. Yang, G.Y. Shen, Y.P. He, X.X. Liu, S.J. Yang, Preparation of TiO2/SiO2 composite oxide and its photocatalytic degradation of rhodamine B, J. Porous Mater. 23 (2016) 589–599, https://doi.org/10.1007/s10934-015-0114-7.

[34] Q. Guo, C. Zhou, Z. Ma, X. Yang, Fundamentals of TiO2 photocatalysis: Concepts, mechanisms, and challenges, Adv. Mater. 31 (2019), https://doi.org/10.1002/adma.201901997.

[35] S.K. Loeb, P.J.J. Alvarez, J.A. Brame, E.L. Cates, W. Choi, J. Crittenden, D. D. Dionysiou, Q. Li, G. Li-Puma, X. Quan, D.L. Sedlak, T. David Waite, P. Westerhoff, J.H. Kim, The technology horizon for photocatalytic water treatment: sunrise or sunset? Environ. Sci. Technol. 53 (2019) 2937–2947, https://doi.org/10.1021/acs.est.8b05041.

[36] M.R. Al-Mamun, S. Kader, M.S. Islam, M.Z.H. Khan, Photocatalytic activity improvement and application of UV-TiO2 photocatalysis in textile wastewater treatment: A review, J. Environ. Chem. Eng. 7 (2019), https://doi.org/10.1016/j.jece.2019.103248.

[37] D. Chen, Y. Cheng, N. Zhou, P. Chen, Y. Wang, K. Li, S. Huo, P. Cheng, P. Peng, R. Zhang, L. Wang, H. Liu, Y. Liu, R. Ruan, Photocatalytic degradation of organic pollutants using TiO2-based photocatalysts: A review, J. Clean Prod. 268 (2020), https://doi.org/10.1016/j.jclepro.2020.121725.

[38] W. Stöber, A. Fink, Controlled growth of monodisperse silica spheres in the micron size range, J. Colloid Interface Sci. 26 (1968) 62–69, https://doi.org/10.1109/ICOSP.2006.345929.

[39] R.F. Egerton, Physical principles of electron microscopy, Springer (2005), https://doi.org/10.1007/b136495.

[40] I. Djerdj, A.M. Tonejc, Structural investigations of nanocrystalline TiO2 samples, J. Alloys Compd. 413 (2006) 159–174, https://doi.org/10.1016/j.jallcom.2005.02.105.

[41] D.T. Cromer, K. Herrington, The structures of anatase and rutile, J. Am. Chem. Soc. 77 (1955) 4708–4709, https://doi.org/10.1021/ja01623a004.

[42] A. Babyszko, A. Wanag, E. Kusiak-Nejman, A.W. Morawski, Effect of calcination temperature of SiO2/TiO2 photocatalysts on UV-VIS and VIS removal efficiency of color contaminants, Catalysts 13 (2023), https://doi.org/10.3390/catal13010186.

[43] S. Musić, N. Filipović-Vinceković, L. Sekovanić, Precipitation of amorphous SiO2 particles and their properties, 28 (n.d.) 89–94. http://www.abeq.org.br/bjche.

[44] C.F. Holder, R.E. Schaak, Tutorial on powder X-ray diffraction for characterizing nanoscale materials, ACS Nano 13 (2019) 7359–7365, https://doi.org/10.1021/acsnano.9b05157.

[45] J.S.J. Hargreaves, Some considerations related to the use of the Scherrer equation in powder X-ray diffraction as applied to heterogeneous catalysts, Catal. Struct. React. 2 (2016) 33–37, https://doi.org/10.1080/2055074X.2016.1252548.
[46] P. Scherrer, P. Debye, Werk Übergeordnetes Werk, Nachr. Ges. Wiss. Göttingen, Math.-Physik. Klasse. 2 (1918) 101–120. http://eudml.org/doc/59018.
[47] U. Holzwarth, N. Gibson, The Scherrer equation versus the "Debye-Scherrer equation", Nat. Nanotechnol. 6 (2011) 534, https://doi.org/10.1038/nnano.2011.145.
[48] W. Su, J. Zhang, Z. Feng, T. Chen, P. Ying, C. Li, Surface phases of TiO2 nanoparticles studied by UV raman spectroscopy and FT-IR spectroscopy, J. Phys. Chem. C 112 (2008) 7710–7716, https://doi.org/10.1021/jp7118422.
[49] S. Brunauer, P.H. Emmett, E. Teller, Adsorption of Gases in Multimolecular Layers, 1938. https://pubs.acs.org/sharingguidelines.
[50] G. Leofanti, M. Padovan, G. Tozzola, B. Venturelli, Surface area and pore texture of catalysts, Catal Today. 41 (1998) 207–219, https://doi.org/10.1016/S0920-5861(98)00050-9.
[51] D. Sun, S. Kang, C. Liu, Q. Lu, L. Cui, B. Hu, Effect of zeta potential and particle size on the stability of SiO2 nanospheres as carrier for ultrasound imaging contrast agents, Int. J. Electrochem. Sci. 11 (2016) 8520–8529, https://doi.org/10.20964/2016.10.30.
[52] T.C. Long, N. Saleh, R.D. Tilton, G.V. Lowry, B. Veronesi, Titanium dioxide (P25) produces reactive oxygen species in immortalized brain microglia (BV2): Implications for nanoparticle neurotoxicity, Environ Sci Technol. 40 (2006) 4346–4352, https://doi.org/10.1021/es060589n.
[53] J.F. Guayaquil-Sosa, B. Serrano-Rosales, P.J. Valadés-Pelayo, H. de Lasa, Photocatalytic hydrogen production using mesoporous TiO2 doped with Pt, Appl. Catal. B. 211 (2017) 337–348, https://doi.org/10.1016/j.apcatb.2017.04.029.
[54] A. Bojinova, R. Kralchevska, I. Poulios, C. Dushkin, Anatase/rutile TiO2 composites: Influence of the mixing ratio on the photocatalytic degradation of Malachite Green and Orange II in slurry, Mater Chem Phys. 106 (2007) 187–192, https://doi.org/10.1016/j.matchemphys.2007.05.035.
[55] B. van Driel, A. Artesani, K.J. van den Berg, J. Dik, S. Mosca, B. Rossenaar, J. Hoekstra, A. Davies, A. Nevin, G. Valentini, D. Comelli, New insights into the complex photoluminescence behaviour of titanium white pigments, Dyes Pigm. 155 (2018) 14–22, https://doi.org/10.1016/j.dyepig.2018.03.012.
[56] K.V. Baiju, A. Zachariah, S. Shukla, S. Biju, M.L.P. Reddy, K.G.K. Warrier, Correlating photoluminescence and photocatalytic activity of mixed-phase nanocrystalline titania, Catal. Lett. 130 (2009) 130–136, https://doi.org/10.1007/s10562-008-9798-5.
[57] L. Zhang, W. Yu, C. Han, J. Guo, Q. Zhang, H. Xie, Q. Shao, Z. Sun, Z. Guo, Large scaled synthesis of heterostructured electrospun TiO2/SnO2 nanofibers with an enhanced photocatalytic activity, J Electrochem Soc. 164 (2017) H651, https://doi.org/10.1149/2.1531709jes.
[58] D.K. Pallotti, L. Passoni, P. Maddalena, F. Di Fonzo, S. Lettieri, Photoluminescence mechanisms in anatase and rutile TiO2, J. Phys. Chem. C 121 (2017) 9011–9021, https://doi.org/10.1021/acs.jpcc.7b00321.
[59] L. Jing, B. Xin, F. Yuan, L. Xue, B. Wang, H. Fu, Effects of surface oxygen vacancies on photophysical and photochemical processes of Zn-doped TiO2 nanoparticles and their relationships, J. Phys. Chem. B 110 (2006) 17860–17865, https://doi.org/10.1021/jp063148z.
[60] J. Nowotny, Titanium dioxide-based semiconductors for solar-driven environmentally friendly applications: Impact of point defects on performance, Energy Environ. Sci. 1 (2008) 565–572, https://doi.org/10.1039/b809111k.
[61] J. Wang, D.N. Tafen, J.P. Lewis, Z. Hong, A. Manivannan, M. Zhi, M. Li, N. Wu, Origin of photocatalytic activity of Nitrogen-doped TiO2 nanobelts, J Am Chem Soc. 131 (2009) 12290–12297, https://doi.org/10.1021/ja903781h.
[62] T.H. Xie, J. Lin, Origin of photocatalytic deactivation of TiO2 film coated on ceramic substrate, J. Phys. Chem. C 111 (2007) 9968–9974, https://doi.org/10.1021/jp072334h.
[63] G. Wang, H. Wang, Y. Ling, Y. Tang, X. Yang, R.C. Fitzmorris, C. Wang, J.Z. Zhang, Y. Li, Hydrogen-treated TiO2 nanowire arrays for photoelectrochemical water splitting, Nano Lett. 11 (2011) 3026–3033, https://doi.org/10.1021/nl201766h.
[64] M. Vasilopoulou, A.M. Douvas, D.G. Georgiadou, L.C. Palilis, S. Kennou, L. Sygellou, A. Soultati, I. Kostis, G. Papadimitropoulos, D. Davazoglou, P. Argitis, The influence of hydrogenation and oxygen vacancies on molybdenum oxides work function and gap states for application in organic optoelectronics, J. Am. Chem. Soc. 134 (2012) 16178–16187, https://doi.org/10.1021/ja3026906.
[65] Y. Lei, L.D. Zhang, G.W. Meng, G.H. Li, X.Y. Zhang, C.H. Liang, W. Chen, S. X. Wang, Preparation and photoluminescence of highly ordered TiO2 nanowire arrays, Appl. Phys. Lett. 78 (2001) 1125–1127, https://doi.org/10.1063/1.1350959.
[66] B. Choudhury, M. Dey, A. Choudhury, Shallow and deep trap emission and luminescence quenching of TiO2 nanoparticles on Cu doping, Applied Nanoscience (Switzerland). 4 (2014) 499–506, https://doi.org/10.1007/s13204-013-0226-9.
[67] N.D. Abazović, M.I. Čomor, M.D. Dramićanin, D.J. Jovanović, S.P. Ahrenkiel, J. M. Nedeljković, Photoluminescence of anatase and rutile TiO2 particles, J. Phys. Chem. B 110 (2006) 25366–25370, https://doi.org/10.1021/jp064454f.
[68] J. Wang, P. Liu, X. Fu, Z. Li, W. Han, X. Wang, Relationship between oxygen defects and the photocatalytic property of zno nanocrystals in nafion membranes, Langmuir 25 (2009) 1218–1223, https://doi.org/10.1021/la803370z.
[69] J. Liqiang, Q. Yichun, W. Baiqi, L. Shudan, J. Baojiang, Y. Libin, F. Wei, F. Honggang, S. Jiazhong, Review of photoluminescence performance of nano-sized semiconductor materials and its relationships with photocatalytic activity, Sol. Energy Mater. Sol. Cells 90 (2006) 1773–1787, https://doi.org/10.1016/j.solmat.2005.11.007.
[70] X. Pan, M.Q. Yang, X. Fu, N. Zhang, Y.J. Xu, Defective TiO2 with oxygen vacancies: Synthesis, properties and photocatalytic applications, Nanoscale 5 (2013) 3601–3614, https://doi.org/10.1039/c3nr00476g.
[71] T.C. Jagadale, S.P. Takale, R.S. Sonawane, H.M. Joshi, S.I. Patil, B.B. Kale, S. B. Ogale, N-doped TiO2 nanoparticle based visible light photocatalyst by modified peroxide sol-gel method, J. Phys. Chem. C 112 (2008) 14595–14602, https://doi.org/10.1021/jp803567f.
[72] M. Kong, Y. Li, X. Chen, T. Tian, P. Fang, F. Zheng, X. Zhao, Tuning the relative concentration ratio of bulk defects to surface defects in TiO2 nanocrystals leads to high photocatalytic efficiency, J. Am. Chem. Soc. 133 (2011) 16414–16417, https://doi.org/10.1021/ja207826q.
[73] R. Schaub, P. Thostrup, N. Lopez, E. Lægsgaard, I. Stensgaard, J.K. Nørskov, F. Besenbacher, Oxygen vacancies as active sites for water dissociation on rutile TiO2(110), Phys Rev Lett. 87 (2001), https://doi.org/10.1103/PhysRevLett.87.266104, 266104-1–266104–4.
[74] K. Yu, L.L. Lou, S. Liu, W. Zhou, Asymmetric oxygen vacancies: the intrinsic redox active sites in metal oxide catalysts, Adv. Sci. 7 (2020) 1–8, https://doi.org/10.1002/advs.201901970.
[75] T. Sekiya, K. Ichimura, M. Igarashi, S. Kurita, Absorption spectra of anatase TiO2 single crystals heat-treated under oxygen atmosphere, J. Phys. Chem. Solid 61 (2000) 1237–1242, https://doi.org/10.1016/S0022-3697(99)00424-2.